Journal of Physics:
Condensed Matter

PAPER • **OPEN ACCESS**

Effect of different crystallographic properties on the electrical conductivity of two polymorphs of a spin crossover complex

To cite this article: Rifat Mahbub *et al* 2025 *J. Phys.: Condens. Matter* **37** 085302

OPEN ACCESS
IOP Publishing
Journal of Physics: Condensed Matter
J. Phys.: Condens. Matter **37** (2025) 085302 (8pp)
https://doi.org/10.1088/1361-648X/ad9a81

Effect of different crystallographic properties on the electrical conductivity of two polymorphs of a spin crossover complex

Rifat Mahbub[1], Kayleigh A McElveen[2], M Zaid Zaz[3], Thilini K Ekanayaka[3], Esha Mishra[3,4], Eric Bissell[5], Parag Banerjee[5,6], David Shapiro[7], Rebecca Y Lai[2], Peter A Dowben[3] and Jeffrey E Shield[1,*]

[1] Department of Mechanical and Materials Engineering, University of Nebraska-Lincoln, 900 N 16th St., Lincoln, NE 68588, United States of America
[2] Department of Chemistry, University of Nebraska-Lincoln, 639 N 12th St., Lincoln, NE 68588, United States of America
[3] Department of Physics and Astronomy, University of Nebraska-Lincoln, 855 N 16th St., Lincoln, NE 68588, United States of America
[4] Department of Physics, Berry College, 2277 Martha Berry Hwy. NW., Mount Berry, GA 30149, United States of America
[5] Department of Materials Science and Engineering, University of Central Florida, Orlando, Orlando, FL 32816, United States of America
[6] Renewable Energy and Chemical Transformations (REACT) Faculty Cluster Initiative, University of Central Florida, Orlando, FL 32816, United States of America
[7] Advanced Light Source, Lawrence Berkeley National Laboratory, Berkeley, CA 94720, United States of America

E-mail: jshield@unl.edu

Received 20 September 2024, revised 18 November 2024
Accepted for publication 4 December 2024
Published 12 December 2024

Abstract

In this study, the structure and transport properties of two polymorphs, nanoparticles and nanorods, of the iron(II) triazole $[Fe(Htrz)_2(trz)](BF_4)$ spin crossover complex were compared. Conductive atomic force microscopy was used to map the electrical conductivity of individual nanoparticles and nanorods. The $[Fe(Htrz)_2(trz)](BF_4)$ nanorods showed significantly higher conductivity compared to nanoparticles. This difference in electrical conductivity is partially associated to the different Fe–N bond lengths in each of the polymorphs, with an inverse relationship between Fe–N bond length and conductivity. Transport measurements were done on the nanorods for both high spin (at 380 K) and low spin (at 320 K) states under dark and illuminated conditions. The conductance is highest for the low spin state under dark conditions. In illumination, the conductance change is much diminished.

* Author to whom any correspondence should be addressed.

Keywords: spin crossover complex, electrical conductivity, thermal hysteresis, nanoparticles, nanorods

1. Introduction

In recent years, a significant amount of research has been directed toward spin crossover complexes due to their unique properties [1, 2], which are characterized by having both high spin and low spin states. These complexes exhibit a reversible transition between these two electronic states, with changing temperature and other various external stimuli including pressure, electric field, and light [1–5]. The two spin states have different magnetic and optical properties, as well as different dielectric constants, color, and configurations. The electrical conductivity of spin crossover complexes is of great interest due to their potential applications in various electronic devices, such as switches [6–8], sensors [9], and memory [8, 10–12] devices. There are several factors [6] which influence the electrical conductivity of spin crossover complexes, although the spin state of the complex is significant [8, 13]. The intermolecular interactions, the crystal structure of the complex and the nature of ligands also play a vital role in determining the conductivity of a spin crossover complex and different crystal structures can be observed at different morphologies [14]. For instance, polymorphism can have different impact on different properties [15] in these materials including conductivity. The study of polymorphism in spin crossover complexes can provide insight into the relationship between the crystal structure and the spin switching in those materials [16–19]. Many previous studies have investigated the influence of polymorphism on spin switching in different spin crossover systems [17–21]. These studies were mainly focused on the crystal structures and magnetic properties of different polymorphs, although a few of them reported the effect of pressure on different polymorphs.

The overall conductivity of $[Fe(Htrz)_2(trz)](BF_4)$ has been well studied [6, 8, 10, 11, 22–27], whose low resistance state has been seen to be either the high spin [21, 23–26] or low spin states [10, 11, 13, 20, 22], making $[Fe(Htrz)_2(trz)](BF_4)$ an interesting system in which to study conductance. Spatial maps of conductance were not a part of prior investigations, however, nor was the effect of different polymorph on the conductance compared. In this study, the electrical conductivity of two morphologies, nanorods and nanoparticles of iron(II) triazole spin crossover complex $[Fe(Htrz)_2(trz)](BF_4)$, was studied.

2. Experimental

The synthesis method for $[Fe(Htrz)_2(trz)](BF_4)$ nanoparticles was adapted from Kroeber *et al* [28]. A 3 M solution of 1,2,4-traizole in anhydrous ethanol was prepared and added at 30 μl min^{-1} using a syringe pump to a solution of 0.5 M $Fe(BF_4)_2 \cdot 6H_2O$ in anhydrous ethanol while stirring. The pale pink solution that resulted was stirred for an additional hour at room temperature before being left overnight. The supernatant was removed, and the resulting solid was collected via gravity filtration and washed with anhydrous ethanol several times.

To prepare the nanorods, micellar mixture 1 was prepared with 360 mg $Fe(BF_4)_2 \cdot 6H_2O$ and 10 mg ascorbic acid in 1 ml nanopure water and is stirred until dispersed. Micellar mixture 2 is prepared by adding 220 mg of 1,2,4-triazole to 1 ml nanopure water and is stirred until dispersed. 8 g Tergitol NP9 is added to each micellar solutions, and both solutions are stirred separately at 60 °C for 5 min. The two solutions are quickly combined and allowed to react while stirring for 24 h. The reaction is stopped with ethyl acetate, and the resulting nanorods are separated via ultracentrifugation at 4500 rpm for 30 min three times using ethyl acetate. This synthesis method was adapted from a previous study by Blanco *et al* [29].

SEM was done on both the nanoparticles and nanorods using FEI Helios NanoLab 660. Nanoparticles and nanorods were dispersed in ethanol individually before dropcasting on carbon tape attached to the sample stage prior to imaging.

Infrared analysis was collected using a Nicolet iS50 Fourier Transform Infrared (FTIR) spectrometer with a SmartPerformer attenuated total reflectance (ATR) accessory with a diamond crystal.

X-ray diffraction was done on both the nanoparticle and nanorod powder using a Rigaku SmartLab diffractometer with Cu-Kα radiation. The diffraction was done from 5° to 50° scattering angle. Rietveld refinement was done on the diffraction patterns using Maud software [30].

The ptychography images of $[Fe(Htrz)_2(trz)](BF_4)$ (Fe-triazole, Htrz = 1 H-1,2,4-triazole and trz = deprotonated triazolato (−) ligand) nanorods were acquired at the COSMIC imaging beamline 7.0.1.2 of the Advanced Light Source at the Lawrence Berkeley National Laboratory. Circularly polarized x-rays with an energy of 709.5 eV were employed for the imaging process. The acquisition was carried out in the transmission mode to reveal the crystal facets.

Magnetic susceptibility measurements were accomplished using a VersaLab 3 Tesla cryogen-free vibrating sample magnetometer (VSM) using an applied magnetic field of 1 T from 300 to 400 K at a heating/cooling rate of 3.5 K min^{-1}.

The current-voltage transport measurements were done using nanorods deposited across an prepatterned electrodes, The $[Fe(Htrz)_2(trz)](BF_4)$ nanorods were dispersed in ethanol and then drop casted on prepatterned electrodes from Fraunhofer Institute for Photonic Microsystems (IPMS) with a 10 μm gap between electrodes, as shown in figure 1. These are designed for organic field effect transistor (OFET) fabrication. The prepatterned electrodes were prepared by sonication in acetone, washed with methanol and dried in a dry nitrogen flow. The film was then dried to be free of solvent prior to the device measurements, by annealing gently for an hour to drive off residual solvent. The current-voltage measurement was performed on an OFET at 320 K and 380 K.

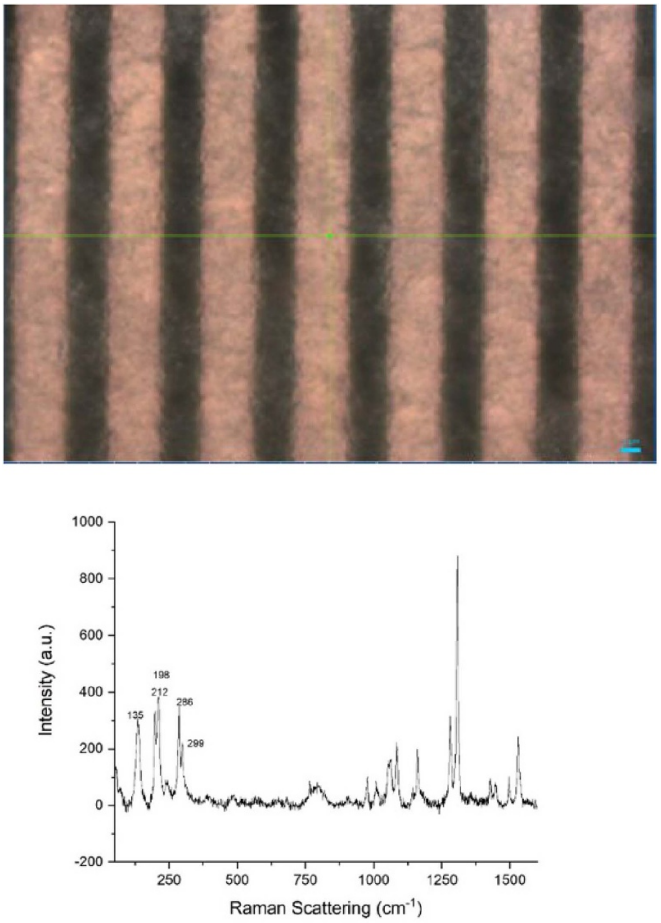

Figure 1. The Raman spectrometry for the $[Fe(Htrz)_2(trz)](BF_4)$ nanorods (bottom) bridging the gap between Fraunhofer institute for photonic microsystems (IPMS) prepatterned electrodes (top). The blue bar, in the lower right hand corner, indicates 2 μm.

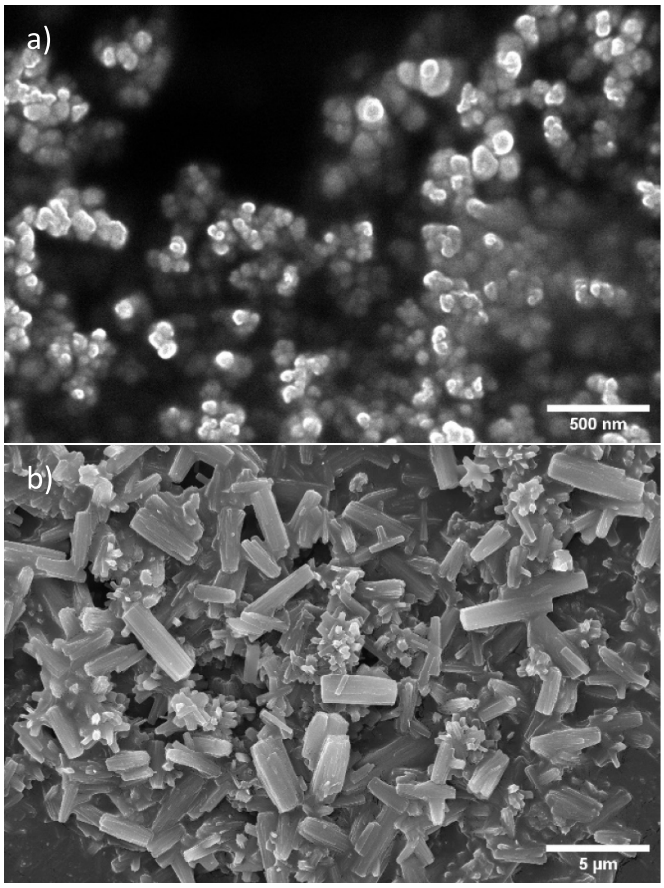

Figure 2. Scanning electron micrographs of $[Fe(Htrz)_2(trz)](BF_4)$ (a) nanoparticles, (b) nanorods.

The data was collected using 4200A-SCS parameter Analyzer and cryogenic lakeshore probe station, both with and without illumination. Transport measurements were done by dropcasting the nanorods suspended in ethanol on prepatterned electrodes and to confirm that the nanorods are indeed bridging the gap between the electrodes. The voltage scan rate was 0.01 V second^{-1}. That the transport measurements reflect only a very small number of bridging $[Fe(Htrz)_2(trz)](BF_4)$ nanorods was confirmed by spatial Raman microscopy as well. It is difficult to say the measurements are of only one nanorod, but the spatial Raman confirm the transport measurements were of only a few bridging nanorods at most. Several different samples were measured with little variation in the transport properties. Raman spectroscopy was done at the gold region (figure 1) of the electrodes. Raman spectroscopy of $[Fe(Htrz)_2(trz)](BF_4)$ has been conducted for both powder form, by Faulmann *et al* and for bulk form, by Ould Moussa *et al* [31, 32] Raman spectroscopy can identify the low spin-high spin transition by observing the difference in the spectra between the two states. The main region of interest is between 100 and 400 cm^{-1}, specifically 207, 212, 288, and 302 cm^{-1}, as peaks in this region are characteristic of lattice phonons and metal-ligand vibrations [31]. The collected spectra are in good agreement with previously reported values [31, 32].

In order to map the electrical conductivity of Fe(II) triazole nanoparticles and nanordos, Bruker Dimension SPM with PeakForce TUNA module was used. Nanorods and nanoparticles were dispersed individually in ethanol at a mass ratio of 1:20 (1-part nanoparticles/nanorods, and 20 parts ethanol), and then sonicated for 40 min. 5 μl of each solution was dropcast on a silicon substrate with gold coating. The conductivity of the dropcast films was measured at a DC bias of 2 V. An SCM PIT V2 conductive AFM tip was used. The scan rate was 0.996 Hz.

3. Results and discussions

SEM was used to confirm that desired morphologies, nanoparticles and nanorods, were fabricated (figure 2). Particle size and nanorod characteristics were also analyzed. The nanoparticles had a mean diameter of 88 nm $\pm$ 18 nm and the nanorods had a mean length of 1857 nm $\pm$ 237 nm and mean diameter of 316 nm $\pm$ 57 nm.

The ATR-IR results for the nanoparticles (figure 3(a)) match the expected results from the literature [33, 34]. The large peak at 1064.3 cm^{-1} is attributed to the coordination of the Fe ion around the 1,2,4-triazole ring structure. The

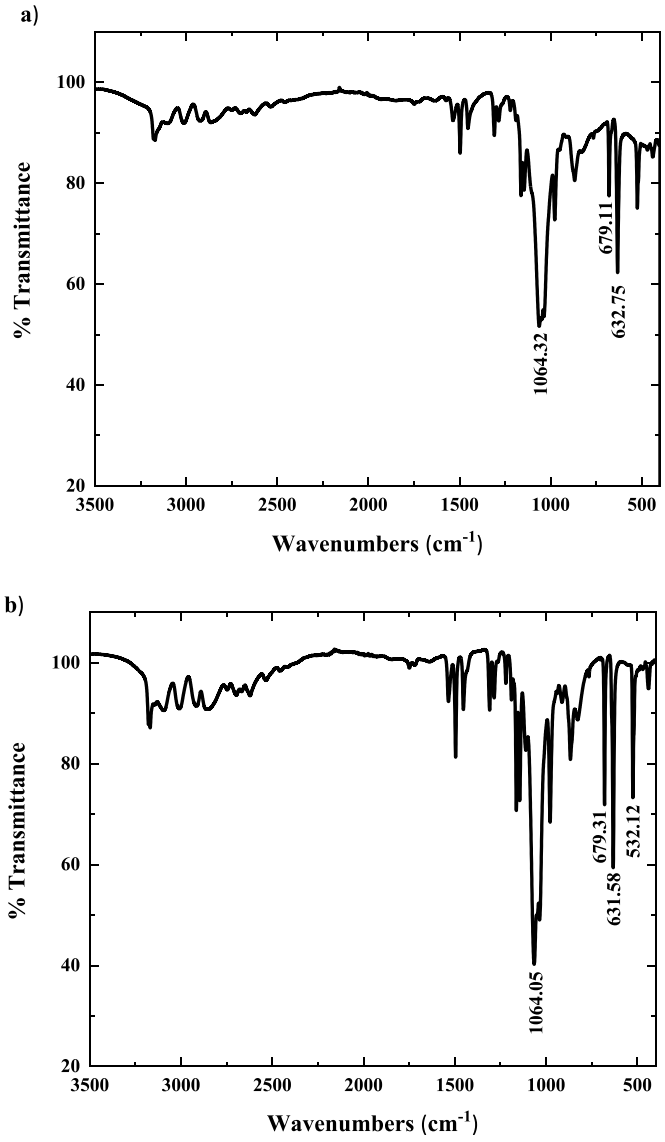

Figure 3. The IR spectra of $[Fe(Htrz)_2(trz)](BF_4)$ (a) nanoparticles, and (b) nanorods.

additional peaks between 3000 and 3100 cm^{-1} are associated with N-H stretching. Haasnoot *et al* [35] previously identified the Htrz and trz ligands using IR spectra assignments, where the absence or reduced intensity of one of the ring torsion vibrations between 600 and 700 cm^{-1} was indicative of both Htrz and trz ligands with C_{2v} symmetry. In the nanoparticles' spectrum, the strong absorption at 632.75 cm^{-1} as well as the less intense absorption at 679.11 cm^{-1} are both indicative of a mixture of Htrz and trz around the Fe(II) center. Similarly, the ATR-IR results for the nanorods (figure 3(b)) can also be compared. The peak at 1064.05 cm^{-1} is also attributed to the coordination of the Fe ion to the 1,2,4-triaozle ring. The peak at 631.58 cm^{-1} and 679.31 cm^{-1} represents the presence of both Htrz and trz ligands around the Fe(II) center. Additional peaks between 3000 and 3100 cm^{-1} are a result of N—H.

The x-ray diffraction results (figure 4) confirmed that both the nanoparticles and nanorods are largely crystalline, as the x-ray diffraction peaks are relatively sharp, and the patterns lack the diffuse scattering characteristic of non-crystalline materials. Rietveld refinement was used to better analyze the diffraction data on the two structures. The refinement was done by considering a trigonal structure and R-3:H space group as a starting point. Structural parameters were then iterated a few times to fit with the experimental data. The sigma values found for nanoparticles and nanorods were 1.24 and 1.68, respectively, indicating relatively good fits considering the complexities of the crystal structures. The crystallographic details for the two structures are shown in table 1. The structures of both the nanoparticles and nanorods fit well into the trigonal space groups. While the unit cell volumes are relatively similar (within ∼10%), the lattice parameters were dramatically different (table 1), with the nanoparticles having a much larger *c*-axis (∼2x) and the nanorods a larger *a*-axis. Another interesting aspect about the structures of the two polymorphs is the Fe–N bond distances, where the average Fe–N bond length was 23.4% shorter for the nanorods. The Scherrer equation was used to calculate coherence lengths. Using the most intense peak, the coherence lengths were calculated to be 32 nm and 47 nm for nanoparticles and nanorods, respectively. These are much smaller than the nanoparticle and nanorod dimensions, suggesting that they are polycrystalline or contain crystalline domains. In spite of these pronounced differences in crystallography, at room temperature, both the $[Fe(Htrz)_2(trz)](BF_4)$ spin crossover polymer nanoparticles and nanorods are in the low spin state, and exhibit the expected spin state transition, as is evident in the magnetic susceptibility times temperature thermal hysteresis loops discussed below.

The ptychographic images, obtained at the COSMIC beamline, are consistent with both the dimensions and crystallinity of the $[Fe(Htrz)_2(trz)](BF_4)$ nanorods (figure 5) derived from XRD. In figure 5, from the changing contrast from the incidence polarization x-rays at the Fe 2p core threshold, there is evidence of facets within the individual $[Fe(Htrz)_2(trz)](BF_4)$ nanorods, indicative of crystallinity. This crystallinity is consistent with greater coherence lengths determined from XRD for the $[Fe(Htrz)_2(trz)](BF_4)$ nanorods.

Magnetic measurements revealed that the transition temperatures between the low spin (LS) state and high spin (HS) states were somewhat different for the nanoparticles and nanorods (figure 6). For nanoparticles, the transition from LS to HS occurred at 375 K and 367 K for each of two cycles, respectively. For nanorods, this transition occurred at 384 K and 377 K, again for Cycle 1 and Cycle 2. Thetransition back to the LS state upon cooling for the nanoparticles were at 324 K and 323 K for two cycles, respectively, while this transition occurred at 355 K and 353 K for the two cycles for the nanorods. For both morphologies, the Fe triazole $[Fe(Htrz)_2(trz)](BF_4)$ was found to be in the low spin state at room temperature. The nanoparticles start to shift from LS state to HS state at a lower temperature compared to nanorods. The nanoparticles have greater cooperativity among the molecules as compared to the nanorods, as the hysteresis is significantly larger for the nanoparticles, consistent with the XRD and ptychography, as discussed above.

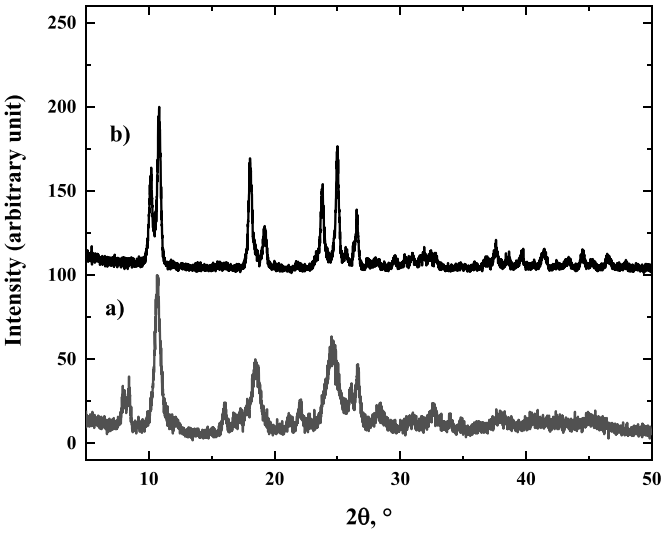

Figure 4. The x-ray diffraction patterns for $[Fe(Htrz)_2(trz)](BF_4)$ (a) nanoparticles, and (b) nanorods.

Table 1. A summary of the crystallographic information of $[Fe(Htrz)_2(trz)](BF_4)$ nanoparticles and nanorods.

	Nanoparticles	Nanorods
Crystal Structure	Trigonal	Trigonal
Space Group	R-3:H	R-3:H
a (Å)	13.22	19.53
c (Å)	48.48	24.98
Average Fe–N bond length (Å)	2.74	2.22

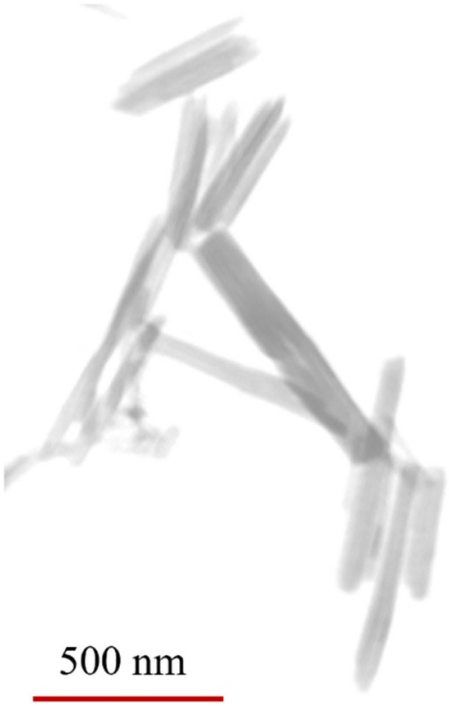

Figure 5. The ptychography image of Fe(II) triazole $[Fe(Htrz)_2(trz)](BF_4)$ nanorods taken using polarized x-rays at the Fe 2p, L3, edge. Note the striped longitudinal contrast along the nanorods.

Conductive atomic force microscopy (c-AFM), as in figure 7, provided both the spatial resolution and measurement sensitivity, to make possible the mapping of the electrical conductivity of individual $[Fe(Htrz)_2(trz)](BF_4)$ nanoparticles and nanorods. The conductivity in the nanoparticles is very low, as shown by the low currents which are on the order of 10^{-15} A (in the femtoampere region). The nanorods, on the other hand, measured currents up to 28 pA, indicating that the $[Fe(Htrz)_2(trz)](BF_4)$ nanorods are more conductive, although the spatially resolved conductivity in these materials is still very low, with measured current only in the picoampere region, while essentially no current was detected down to the femtoampere scale for the nanoparticles—a difference of at least 3 orders of magnitude. (figures 7(b) and (d)). This difference in conductivity may be associated with the different Fe–N bond lengths in these two polymorphs of Fe(II) triazole, as nanoparticles have larger Fe–N bond distances compared to the nanorods. Further, the high spin state is characterized by larger Fe–N bond length, while the low spin state is characterized by smaller Fe–N bond length. Moreover, the samples were exposed to light while doing the AFM experiments. Therefore, it is possible that the illumination caused part of the sample to transform from the LS state to the HS state since the material is photoactive. Further, this effect of illumination will affect the nanoparticles more as they have less a stable LS state.

To further confirm that the $[Fe(Htrz)_2(trz)](BF_4)$ nanorods are more conductive in the low spin state, as has been seen before for nanorods [6, 10, 22, 25, 27], the effect of illumination and spin state on the conductivity was also studied. The experiments were done in both illuminated and dark conditions to determine the effect of illumination on conductivity. The $I(V)$ transport studies were done at 320 K and 380 K, where the iron triazole is in the low and high spin states, respectively. Also, the effect of illumination on the $[Fe(Htrz)_2(trz)](BF_4)$ current versus voltage $I(V)$ characteristics is significant as it causes a transition from the low spin to high spin state at room temperature, as has been previously established [36]. Consequently, transport measurements under both illuminated and dark conditions are revealing. Figure 8 shows the I–V conductance curves of the $[Fe(Htrz)_2(trz)](BF_4)$ nanorods for both the high spin state (380 K) and low spin state (320 K) in both light and dark conditions illustrate that the current on/off ratio is very large when measured in the dark (figure 8(b)) compared to under illumination (figure 8(a)). The low spin state to high spin state currents for $[Fe(Htrz)_2(trz)](BF_4)$ are lower with the light 'on' because $[Fe(Htrz)_2(trz)](BF_4)$ is photoactive, and light will transition low-spin $[Fe(Htrz)_2(trz)](BF_4)$ into the high spin state so the conductance at 320 K decreases, reducing the on/off ratio significantly. The I–V curve shows almost an Ohmic behavior without illumination in the low spin state.

The transport measurements are not done with point contacts nor a break junction, so there is no assurity here that

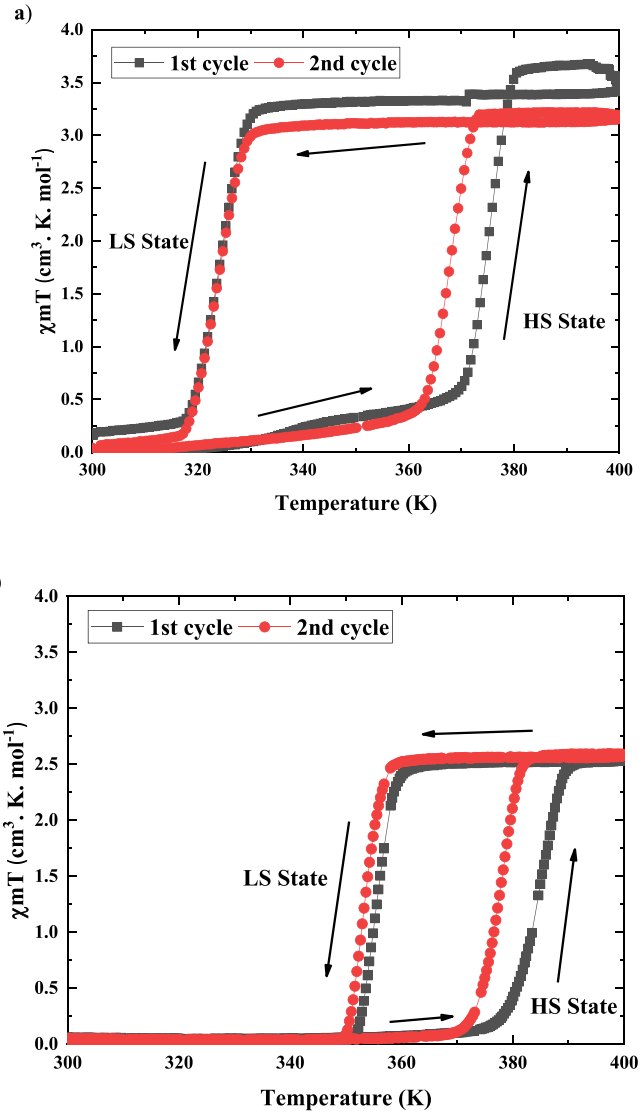

Figure 6. The magnetic susceptibility times temperature thermal hysteresis loops for $[Fe(Htrz)_2(trz)](BF_4)$ (a) nanoparticles, and (b) nanorods.

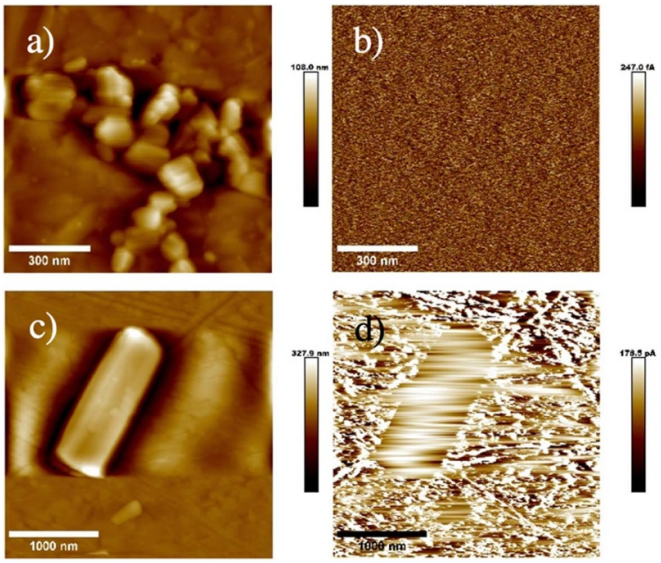

Figure 7. Atomic force microscope images for $[Fe(Htrz)_2(trz)](BF_4)$ nanoparticles and nanorods. (a) Height map image of nanoparticles, (b) electrical conductivity map of nanoparticles, (c) height map of nanorods, and (d) electrical conductivity map of nanorods.

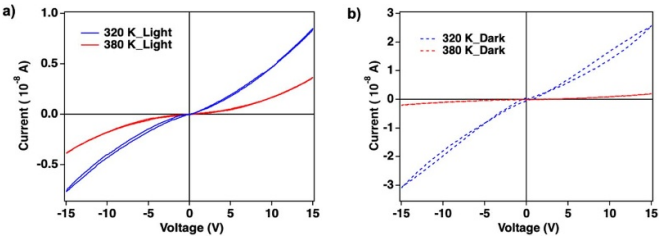

Figure 8. The current-voltage measurements taken for $[Fe(Htrz)_2(trz)](BF_4)$ nanorods in (a) light (fluorescent light) and (b) dark at low spin (320 K) and high spin (380 K) states.

the transport behavior reflects a single $[Fe(Htrz)_2(trz)](BF_4)$ nanorod. Transport measurements through a single $[Fe(Htrz)_2(trz)](BF_4)$ nanoparticle have been reported elsewhere [23, 24], with similar changes in current with spin state. As noted elsewhere [24], it is noted that voltage poling of $[Fe(Htrz)_2(trz)](BF_4)$ nanoparticles does indeed change the photoconductance. This raised a key issue regarding the possible effects of different packing arrangement on the overall conductance. Lattice solvent is known to affect both electrical [37] and thermal conductance [38], as the choice of solvent affects the molecular packing [39, 40].

4. Conclusion

In this study, the effect of morphology on crystal parameters and conductance for the spin crossover iron(II) triazole $[Fe(Htrz)_2(trz)](BF_4)$ complex for two different morphologies (nanoparticles and nanorods) was investigated. Both morphologies were observed to be crystalline but were found to have different crystal structures. While both x-ray diffraction patterns were indexed to the trigonal structure, lattice parameters were significantly different for the nanoparticles versus nanorods. Conductivity experiments on individual nanoparticles and nanorods, accomplished using conductive atomic force microscopy, also revealed different behavior for the nanoparticles and nanorods. The nanorods were found to have much higher conductivity than the nanoparticles when measured using conductive atomic force microscopy. The difference was attributed to the different Fe–N bond length in the two structures. The Fe–N bond length is longer in the $[Fe(Htrz)_2(trz)](BF_4)$ nanoparticles than in the nanorods. Temperature-dependent magnetic analysis revealed thermal hysteresis of the magnetic susceptibility on both $[Fe(Htrz)_2(trz)](BF_4)$ polymorphs, confirming the presence of a spin crossover transition. The temperature range over which the hysteresis occurred was larger for nanoparticles (44 K) than it was for the nanorods (24 K), indicating greater cooperativity for the more crystalline polymorph. In fact, facets can be identified within the

$[Fe(Htrz)_2(trz)](BF_4)$ nanorods. These differences in different behaviors in the polymorphs can also be attributed to their size differences and synthesis technique [10].

Data availability statement

The data cannot be made publicly available upon publication because no suitable repository exists for hosting data in this field of study. The data that support the findings of this study are available upon reasonable request from the authors.

Acknowledgments

This work was supported by the National Science Foundation, Division of Materials Research, Grants NSF-PREM #1827690, and NSF-DMR-EPM 2317464, and EPSCoR RII Track-1: Emergent Quantum Materials and Technologies (EQUATE) 2044049. This research used resources of the Advanced Light Source, which is a DOE Office of Science User Facility under Contract No. DE-AC02-05CH11231. The Raman system used was acquired under the NSF MRI Program Award #1920050. The research was performed in part in the Nebraska Nanoscale Facility: National Nanotechnology Coordinated Infrastructure by the National Science Foundation under Award No. ECCS: 2025298, and with support from the Nebraska Research Initiative through the Nebraska Center for Materials and Nanoscience and the Nanoengineering Research Core Facility at the University of Nebraska-Lincoln.

ORCID iDs

M Zaid Zaz https://orcid.org/0000-0001-7849-4715
Thilini K Ekanayaka https://orcid.org/0000-0003-3650-0210
David Shapiro https://orcid.org/0000-0002-4186-6017
Rebecca Y Lai https://orcid.org/0000-0002-1732-9481
Peter A Dowben https://orcid.org/0000-0002-2198-4710
Jeffrey E Shield https://orcid.org/0000-0002-1415-2115

References

[1] Gütlich P, Garcia Y and Goodwin H A 2000 Spin crossover phenomena in Fe(II) complexes *Chem. Soc. Rev.* **29** 419–27
[2] Nicolazzi W and Bousseksou A 2018 Thermodynamical aspects of the spin crossover phenomenon *C. R. Chim.* **21** 1060–74
[3] Gütlich P, Gaspar A B and Garcia Y 2013 Spin state switching in iron coordination compounds *Beilstein J. Org. Chem.* **9** 342–91
[4] Ridier K, Molnár G, Salmon L, Nicolazzi W and Bousseksou A 2017 Hysteresis, nucleation and growth phenomena in spin-crossover solids *Solid State Sci.* **74** A1–A22
[5] Hauser A, Jeftić J, Romstedt H, Hinek R and Spiering H 1999 Cooperative phenomena and light-induced bistability in iron(II) spin-crossover compounds *Coord. Chem. Rev.* **190–192** 471–91
[6] Zaz M Z, Ekanayaka T K, Cheng R and Dowben P A 2023 Variability of the conductance changes associated with the change in the spin state in molecular spin crossover complexes *Magnetochemistry* **9** 223
[7] Lefter C, Davesne V, Salmon L, Molnár G, Demont P, Rotaru A and Bousseksou A 2016 Charge transport and electrical properties of spin crossover materials: towards nanoelectronic and spintronic devices *Magnetochemistry* **2** 18
[8] Rotaru A, Dugay J, Tan R P, Guralskiy I A, Salmon L, Demont P, Carrey J, Molnár G, Respaud M and Bousseksou A 2013 Nano-electromanipulation of spin crossover nanorods: towards switchable nanoelectronic devices *Adv. Mater.* **25** 1745–9
[9] Ridier K, Bas A-C, Zhang Y, Routaboul L, Salmon L, Molnár G, Bergaud C and Azzedine Bousseksou A 2020 Unprecedented switching endurance affords for high-resolution surface temperature mapping using a spin-crossover film *Nat. Commun.* **11** 3611
[10] Holovchenko A, Dugay J, Giménez-Marqués M, Torres-Cavanillas R, Coronado E and van der Zant H S J 2016 Near room-temperature memory devices based on hybrid spin-crossover@SiO_2 nanoparticles coupled to single-layer graphene nanoelectrodes *Adv. Mater.* **28** 7228–33
[11] Tanaka D *et al* 2019 Facile preparation of hybrid thin films composed of spin-crossover nanoparticles and carbon nanotubes for electrical memory devices *Dalton Trans.* **48** 7074–9
[12] Ekanayaka T K *et al* 2021 Nonvolatile voltage controlled molecular spin state switching for memory applications *Magnetochemistry* **7** 37
[13] Rotaru A, Gural'skiy I A, Molnár G, Salmon L, Demont P and Bousseksou A 2012 Spin state dependence of electrical conductivity of spin crossover materials *Chem. Commun.* **48** 4163–5
[14] Lamichhane S, McElveen K A, Erickson A, Fescenko I, Sun S, Timalsina R, Guo Y, Liou S H, Lai R Y and Laraoui A 2023 Nitrogen-vacancy magnetometry of individual Fe-triazole spin crossover nanorods *ACS Nano* **17** 8694–704
[15] Palluel M, Khoury L A, Daro N, Buffière S, Josse M, Marchivie M and Chastanet G 2021 Rational direct synthesis of $[Fe(Htrz)_2(trz)](BF_4)$ polymorphs: temperature and concentration effects *Inorg. Chem. Front.* **8** 3697–706
[16] Tao J, Wei R-J, Huang R-B and Zheng L-S 2012 Polymorphism in spin-crossover systems *Chem. Soc. Rev.* **41** 703–37
[17] Galet A, Gaspar A B, Muñoz M C, Levchenko G and Real J A 2006 Pressure effect and crystal structure reinvestigations on the spin crossover system: $[Fe(bt)_2(NCS)_2]$ (bt = 2,2'-Bithiazoline) polymorphs A and B *Inorg. Chem.* **45** 9670–9
[18] Matouzenko G S, Bousseksou A, Lecocq S, van Koningsbruggen P J, Perrin M, Kahn O and Collet A 1997 Polymorphism in spin transition systems. crystal structure, magnetic properties, and mössbauer spectroscopy of three polymorphic modifications of $[Fe(DPPA)(NCS)_2]$ [DPPA = (3-Aminopropyl)bis(2-pyridylmethyl)amine] *Inorg. Chem.* **36** 5869–79
[19] Moliner N, Muñoz M C, Létard S, Létard J F, Solans X, Burriel R, Castro M, Kahn O and Real J A 1999 Spin-crossover in the $[Fe(abpt)_2(NCX)_2]$ (X=S, Se) system: structural, magnetic, calorimetric and photomagnetic studies *Inorganica Chim. Acta* **291** 279–88
[20] Sheu C-F, Pillet S, Lin Y-C, Chen S-M, Hsu I-J, Lecomte C and Wang Y 2008 Magnetostructural relationship in the spin-crossover complex t-$\{Fe(abpt)_2[N(CN)_2]_2\}$:

polymorphism and disorder phenomenon *Inorg. Chem.* **47** 10866–74
[21] Dupouy G, Marchivie M, Triki S, Sala-Pala J, Salaün J-Y, Gómez-García C J and Guionneau P 2008 The key role of the intermolecular π−π interactions in the presence of spin crossover in neutral [Fe(abpt)$_2$A$_2$] complexes (A = Terminal Monoanion N Ligand) *Inorg. Chem.* **47** 8921–31
[22] Dugay J, Giménez-Marqués M, Kozlova T, Zandbergen H W, Coronado E and van der Zant H S J 2015 Spin switching in electronic devices based on 2D assemblies of spin-crossover nanoparticles *Adv. Mater.* **27** 1288–93
[23] Prins F, Monrabal-Capilla M, Osorio E A, Coronado E and van der Zant H S J 2011 Room-temperature electrical addressing of a bistable spin-crossover molecular system *Adv. Mater.* **23** 1545–9
[24] Etrillard C, Faramarzi V, Dayen J-F, Letard J-F and Doudin B 2011 Photoconduction in [Fe(Htrz)$_2$(trz)](BF$_4$)·H$_2$O nanocrystals *Chem. Commun.* **47** 9663–5
[25] Chen Y-C, Meng Y, Ni Z-P and Tong M-L 2015 Synergistic electrical bistability in a conductive spin crossover heterostructure *J. Mater. Chem.* C **3** 945
[26] Siddiqui S A, Domanov O, Schafler E, Vejpravova J and Shiozawa H 2021 Synthesis and size-dependent spin crossover of coordination polymer [Fe(Htrz)$_2$(trz)](BF$_4$) *J. Mater. Chem.* C **9** 1077–84
[27] Mishra E, Ekanayaka T K, McElveen K A, Lai R Y and Dowben P A 2022 Evidence for long drift carrier lifetimes in [Fe(Htrz)$_2$(trz)](BF$_4$) plus polyaniline composites *Org. Electron.* **105** 106516
[28] Kroeber J *et al* 1994 Spin transitions and thermal hysteresis in the molecular-based materials [Fe(Htrz)2(trz)](BF4) and [Fe(Htrz)3](BF4)2.cntdot.H2O (Htrz = 1,2,4-4H-triazole; trz = 1,2,4-triazolato) *Chem. Mater.* **6** 1404–12
[29] Blanco A A, Adams D J, Azoulay J D, Spinu L and Wiley J B 2022 Synthesis and characterization of [Fe(Htrz)$_2$(trz)](BF$_4$)] nanocubes *Molecules* **27** 1213
[30] Lutterotti L 1999 MAUD: a friendly Java program for material analysis using diffraction vol 21 pp 14–15 (CPD News Letter) (available at: https://luttero.github.io/maud/maud/release/2023/07/03/new-version-2.999.html)
[31] Faulmann C, Chahine J, Malfant I, de Caro D, Cormary B and Valade L 2011 A facile route for the preparation of nanoparticles of the spin-crossover complex [Fe(Htrz)$_2$(trz)](BF$_4$) in xerogel transparent composite films *Dalton Trans.* **40** 2480–5
[32] Ould Moussa N, Ostrovskii D, Martinez Garcia V, Molnár G, Tanaka K, Gaspar A B, Real J A and Bousseksou A 2009 Bidirectional photo-switching of the spin state of iron(II) ions in a triazol based spin crossover complex within the thermal hysteresis loop *Chem. Phys. Lett.* **477** 156–9
[33] Diaconu A, Lupu S-L, Rusu I, Risca I-M, Salmon L, Molnár G, Bousseksou A, Demont P and Rotaru A 2017 Piezoresistive effect in the [Fe(Htrz)$_2$(trz)](BF$_4$) spin crossover complex *J. Phys. Chem. Lett.* **8** 3147–51
[34] Nguyen T-A D, Veauthier J M, Angles-Tamayo G F, Chavez D E, Lapsheva E, Myers T W, Nelson T R and Schelter E J 2020 Correlating mechanical sensitivity with spin transition in the explosive spin crossover complex [Fe(Htrz)$_3$]$_n$[ClO$_4$]$_{2\ n}$ *J. Am. Chem. Soc.* **142** 4842–51
[35] Haasnoot J G, Vos G and Groeneveld W L 1977 1,2,4-triazole complexes, III complexes of transition metal(II) nitrates and fluoroborates *Z. Naturforsch.* B **32** 1421–30
[36] Ekanayaka T K, Kurz H, McElveen K A, Hao G, Mishra E, N'Diaye A T, Lai R Y, Weber B and Dowben P A 2022 Evidence for surface effects on the intermolecular interactions in Fe(II) spin crossover coordination polymers *Phys. Chem. Chem. Phys.* **24** 883–94
[37] Tiunova A V, Korchagin D V, Kazakova A V, Shilov G V, Buravov L I, Dmitriev A I, Zhidkov M V, Zverev V N, Yagubskii E B and Aldoshin S M 2024 Solvent and dihalide substituent effects on crystal structure, spin-crossover behavior and conductivity of the cationic Mn(III) complexes with electroactive TCNQ counteranions *Eur. J. Inorg. Chem.* **27** e202300749
[38] Rat S, Ridier K, Vendier L, Molnár G, Salmon L and Bousseksou A 2017 Solvatomorphism and structural-spin crossover property relationship in bis[hydrotris(1,2,4-triazol-1-yl)borate]iron(II) *Cryst. Eng. Comm.* **219** 3271
[39] Phonsri W, Harding P, Liu L, Telfer S G, Murray K S, Moubaraki B, Ross T M, Jameson G N L and Harding D J 2017 Solvent modified spin crossover in an iron(III) complex: phase changes and an exceptionally wide hysteresis *Chem. Sci.* **8** 3949
[40] Bas A-C, Shalabaeva V, Thompson X, Vendier L, Salmon L, Thibault C, Molnar G, Routaboul L and Bousseksou A 2019 Effects of solvent vapor annealing on the crystallinity and spin crossover properties of thin films of [Fe(HB(tz)$_3$)$_2$] *C. R. Chim.* **22** 525e533